International Journal of Solids and Structures 46 (2009) 1856–1871

Contents lists available at ScienceDirect

International Journal of Solids and Structures

journal homepage: www.elsevier.com/locate/ijsolstr

Drive level dependency in quartz resonators

Mihir S Patel [a,*], Yook-Kong Yong [a], Masako Tanaka [b]

[a] Civil and Environmental Engineering, Rutgers University, 623 Bowser Road, Piscataway, NJ 08854, USA
[b] R&D Department, Seiko Epson Corporation, Nagano-ken 392-8502, Japan

ARTICLE INFO

Article history:
Received 13 June 2008
Received in revised form 15 December 2008
Available online 14 January 2009

Keywords:
Drive level dependency
Quartz
Power density
Q-factor
Spurious modes

ABSTRACT

Common piezoelectric resonators such as quartz resonators have a very high Q and ultra stable resonant frequency. However, due to small material nonlinearities in the quartz crystal, the resonator is drive level dependent, that is, the resonator level of activity and its frequency are dependent on the driving, or excitation, voltage. The size of these resonators will be reduced to one fourth of their current sizes in the next few years, but the electrical power which is applied will not be reduced as much. Hence, the applied power to resonator size ratio will be larger, and the drive level dependency may play a role in the resonator designs.

We study this phenomenon using the Lagrangian nonlinear stress equations of motion and Piola–Kirchhoff stress tensor of the second kind. Solutions are obtained using COMSOL for the AT-cut, BT-cut, SC-cut and other doubly rotated cut quartz resonators and the results compared well with experimental data. The phenomenon of the drive level dependence is discussed in terms of the voltage drive, electric field, power density and current density. It is found that the drive level dependency is best described in terms of the power density. Experimental results for the AT-, BT- and SC-cut resonators in comparison with our model results are presented. Results for new doubly rotated cuts are presented. The effects of spurious modes, quality factor and air damping on DLD are presented.

© 2009 Elsevier Ltd. All rights reserved.

1. Introduction

The future requirements of frequency control devices are that they be smaller and more stable at higher frequencies. However, with the increasing demand of smaller size it becomes more difficult to design high precision frequency control devices. One of the main causes of frequency instability is the role played by the intrinsic nonlinearities of quartz resonators. These intrinsic nonlinearities are responsible for the coupling between the ultrasonic wave and external or internal quasistatic perturbations. The dependence of the resonator frequency on its drive levels is one of the phenomena caused by the material nonlinearities of quartz. We call this dependency the drive level dependency (DLD).

The drive level dependency corresponds to the amplitude–frequency and the intermodulation effects. The amplitude–frequency effect corresponds to the dependence of the frequency of a resonator on the drive level and appears as a distortion of the amplitude and phase resonance curves. As the drive level (the current through a crystal) increases, the crystal's amplitude of vibration also increases and the effects due to the nonlinearities of quartz become more pronounced. In oscillators the amplitude modulation noise is transformed into short term frequency noise. For the long term all drifts of driving power are converted into frequency drifts; for the same kind of resonators in case of power variations of 1%, to achieve a theoretical frequency stability of more than parts per million, the mean driving power has to be almost as low as a few mW (Gagnepain et al., 1977). Thus, non-linear amplitude–frequency effect is a limiting factor for their use at high drive level in oscillators and resonators.

When the driving signal is composed of two nearby frequencies, intermodulation is generated by the crystal nonlinearities if the driving powers are moderately high. It also appears that intermodulation can also be attributed to some surface effects corresponding to mechanical and electrical defects. The nonlinearities are also responsible for the coupling between different vibration modes of the resonator. This is a phenomenon which can lead to "activity dips", and must be distinguished from linear coupling due to piezoelectric excitation and thermal sensitivities of different modes. The sensitivity of mode coupling to power level is characteristic of non-linear coupling.

Several experiments have been carried in order to investigate the nonlinear resonance of AT-cut quartz resonators by Warner (Warner, 1959), and Wood and Seed (Wood and Seed, 1967) by using amplitude-resonance curve methods. However, the limitations of the method involved in determining the amplitude–frequency effect did not gave an accurate picture of how the nonlinearities affected the drive-level of the resonators. Later work was carried out by Tiersten (Tiersten, 1974; Tiersten, 1975; Tiersten, 1975) who derived the nonlinear differential equations

* Corresponding author. Tel.: +1 9088123735.
E-mail address: patelmihirs@gmail.com (M.S Patel).

0020-7683/$ - see front matter © 2009 Elsevier Ltd. All rights reserved.
doi:10.1016/j.ijsolstr.2008.12.021

and boundary conditions containing terms up to cubic in the small field variables from general nonlinear electrostatic equation. The equations were helpful in determining the fourth order elastic constant C_{6666} which gives a good approximation of the theoretical results to that of the experimental results. Further, these equations proved that the amplitude–frequency effect in quartz resonators is due to the intrinsic material nonlinearities. For the past few years extensive research has been carried out in determining the drive level dependence of quartz oscillator, but due to the assumptions used in order to simplify the cumbersome nonlinear equations, it becomes increasingly difficult to obtain valid analytical results for comparison with the experimental results.

We have developed an accurate 3-D finite element model, which can predict the drive level dependence of a quartz resonator. The drive level dependency of AT-cut, SC-cut, BT-cut obtained from the FE model compares well with the experimental results. Also, the drive level dependencies of different cuts are also predicted. Here, we also show that the drive level expressed as the power density, rather than say the voltage drive level, is the most suitable parameter for describing the effects of the DLD.

Further, the DLD effect is studied with respect to energy dissipation due to the support mountings and material dissipation. The effect of DLD on the quality factor of quartz resonators could be found.

2. Nonlinear governing equations

The crystal is referred to a Cartesian coordinate system x_1, x_2, x_3, with the x_2-axis normal to the major surface of the rotated quartz cuts. The governing equations which define the effects of intrinsic nonlinearities on the thickness shear vibrations of a piezoelectric resonator with material losses corresponding to the mechanical damping and resistance in current conduction (Yong et al., 2007) are as follows:

Non-linear strain-displacement relationships:

$$E_{ij} = \frac{1}{2}(U_{i,j} + U_{j,i} + U_{k,i}U_{k,j}) \tag{1}$$

Non-linear stress-strain relationships:

$$T_{ij} = C_{ijkl}E_{kl} + \frac{1}{2}C_{ijklmn}E_{kl}E_{mn} + e_{pij}\phi_{,p} + \eta_{ijkl}\dot{E}_{kl} \tag{2}$$

Linear electrostatics relationships:

$$D_i = e_{ikl}E_{kl} - \varepsilon_{ip}\phi_{,p}, \quad J_i = -\sigma_{ik}\phi_{,k} \tag{3}$$

Non-linear stress equation of motion:

$$(T_{ij} + T_{jk}U_{i,k})_{,j} = \rho\ddot{U}_i \tag{4}$$

Charge equation of electrostatics:

$$\dot{D}_{i,i} + J_{i,i} = 0 \tag{5}$$

In the above set of equations, E_{ij} is the strain tensor, T_{ij} is stress tensor, C_{ijkl} and C_{ijklmn} are the second and third order elastic constants, respectively, e_{pij} is the piezoelectric coefficient, ε_{ip} is the dielectric permittivity, η_{ijkl} is the acoustic viscosity tensor, σ_{ik} is the electric conductivity, J_i is the conduction current, D_i is the electric displacement, and $\phi_{,p}$ is the electric field intensity vector. Eqs. (4.1) to (4.5) form a system of 25 equations with 25 unknowns ($6T_{ij}$, $6E_{ij}$, $3U_i$, $3\phi_{,p}$, $3D_i$, $3J_i$ and $1\phi_p$). It should be noted that the viscosity tensor η_{ijkl} has the same symmetry as the elasticity tensor C_{ijkl}, and the conductivity tensor σ_{ik} the symmetry as the permittivity tensor ε_{ip} (Lamb and Richter, 1966). The material parameters C_{ijkl}, e_{pij} and ε_{ip} for quartz are obtained from (Hellwedge and Hellwedge, 1966), η_{ijkl}, C_{ijklmn} and σ_{ik} are obtained from (Lamb and Richter, 1966; Thurston et al., 1966; Lee et al., 2004), respectively. These constants are rotated about the respective axes to obtain the numerical values for different cuts (e.g. AT-Cut).

In the case in which the bounding surface S is in contact with free space, the boundary conditions are:

$$n_i T_{ij} = \hat{t}_j \text{ or } u_j = \widehat{u}_j, \tag{6}$$

$$n_i[\dot{D}_i + J_i] = \dot{q}_i \text{ or } [\phi] = \hat{\phi} \tag{7}$$

where, n_i is the outward unit normal of S, $\hat{t}_j$ and $\hat{u}_j$ are the specified traction and displacement, respectively. For the unelectroded quartz surfaces, $\dot{q}_i = 0$. In the case in which the surface S is in contact with a shorted electrode

$$[\phi] = 0 \tag{8}$$

After a solution of the governing Eqs. (1)–(5) is obtained, the surface current density $\dot{q}_i$ at S under the electrode can be computed by:

$$n_i[\dot{D}_i + J_i] = \dot{q}_i \tag{9}$$

In order to define the nonlinear effect due to the drive level, it was necessary to develop a model which incorporates the quasistatic deformations coupling with that of the higher order elastic constants. However, it was not possible to directly establish a relationship between the higher order nonlinear strain terms and the third order elastic constants. Thus the theoretical analysis can be simplified by considering that the wave has small amplitude. Therefore only the modification of the wave characteristics by the predeformation are considered and the influence of the wave on the predeformation can be neglected. This will linearize the nonlinear governing equations.

The influence of the intermodulation effects due to fourth order elastic constants was neglected in our current study. Also, the drive level effect of quartz resonators was predominantly affected by the higher order mechanical nonlinearities rather than those of the piezoelectric constants. Hence, the higher order piezoelectric constants are not taken into account.

An iterative algorithm is developed in order to model the drive level effect as follows:

STEP 1: Obtain the stresses and strains $\widetilde{T}_{ij}, \widetilde{U}_{i,j}$ at the thickness shear mode of interest using the forced vibrations frequency response solution to the linear governing equations below. The damping in the forced vibration model is taken into account by the acoustic viscosity tensor. The resonance frequency of interest is first identified in a linear eigenvalue problem solution.

$$\begin{aligned}
&\widetilde{E}_{ij} = \frac{1}{2}(\widetilde{U}_{j,i} + \widetilde{U}_{i,j}) \\
&\widetilde{T}_{ij} = C_{ijkl}\widetilde{E}_{kl} + e_{pij}\phi_{,p} + \eta_{ijkl}\dot{E}_{kl} \\
&D_i = e_{ikl}\widetilde{E}_{kl} - \varepsilon_{ip}\phi_{,p} \\
&\widetilde{T}_{ij,j} = \rho\ddot{\widetilde{U}}_i \\
&\dot{D}_{i,i} + J_{i,i} = 0
\end{aligned} \tag{10}$$

STEP 2: Substitute the stresses and strains $\widetilde{T}_{ij}, \widetilde{U}_{i,j}$ from STEP 1 into the nonlinear governing equations below. Please note however that the nonlinear parts of the equations are replaced by the stresses and strains $\widetilde{T}_{ij}, \widetilde{U}_{i,j}$ from STEP 1. Solve for the forced vibrations frequency response and obtain the response stresses and strains $\widehat{T}_{ij}, \widehat{U}_{i,j}$.

$$\begin{aligned}
&\widehat{E}_{ij} = \frac{1}{2}(\widehat{U}_{j,i} + \widehat{U}_{i,j} + \widetilde{U}_{k,i}\widetilde{U}_{k,j}) \\
&\widehat{T}_{ij} = C_{ijkl}\widehat{E}_{kl} + \frac{1}{2}C_{ijklmn}\widehat{E}_{kl}\widetilde{E}_{mn} + e_{pij}\phi_{,p} + \eta_{ijkl}\dot{\widehat{E}}_{kl} \\
&D_i = e_{ikl}\widehat{E}_{kl} - \varepsilon_{ip}\phi_{,p} \\
&(\widehat{T}_{ij} + \widetilde{T}_{jk}\widetilde{U}_{i,k})_{,j} = \rho\ddot{\widehat{U}}_i \\
&\dot{D}_{i,i} + J_{i,i} = 0
\end{aligned} \tag{11}$$

STEP 3: Use the stresses and strains $\widehat{T}_{ij}, \widehat{U}_{i,j}$ and substitute into the nonlinear governing equations below. Solve for the forced vibrations frequency response stresses and strains $\breve{T}_{ij}, \breve{U}_{i,j}$.

$$\begin{aligned}
&\breve{E}_{ij} = \frac{1}{2}(\breve{U}_{j,i} + \breve{U}_{i,j} + \widehat{U}_{k,i}\widehat{U}_{k,j}) \\
&\breve{T}_{ij} = C_{ijkl}\breve{E}_{kl} + \frac{1}{2}C_{ijklmn}\breve{E}_{kl}\widehat{E}_{mn} + e_{pij}\phi_{,p} + \eta_{ijkl}\dot{\breve{E}}_{kl} \\
&D_i = e_{ikl}E_{kl} - \varepsilon_{ip}\phi_{,p} \\
&(\breve{T}_{ij} + \widehat{T}_{jk}\widehat{U}_{i,k})_{,j} = \rho\ddot{\breve{U}}_i \\
&\dot{D}_{i,i} + J_{i,i} = 0
\end{aligned} \tag{12}$$

STEP 4: Iterate between STEP 2 and STEP 3 until a stable resonance frequency is obtained.

3. Finite element simulation and comparison with experimental results

There are different commercially available finite element software's such as ANSYS, ANSOFT, ABAQUS, and the list continues. ANSYS is one of the most commonly used finite element software used in the industry. However, the disadvantage of the above mentioned finite element software package's is their inability to let the user modify the equation of motion so as to introduce the nonlinear iterative algorithm mentioned above. COMSOL 3.3 is a finite element software package which evolved from the partial differential toolbox in MATLAB to a full finite element software package, gives user the flexibility to write their own partial differential equations and modify the equations of motion. Thus, the above iterative algorithm was implemented in COMSOL 3.3 to simulate the drive level effect in various quartz resonators by using frequency response analysis. FE calculations for different drive levels varying from 0.0001 to 10 V shows that the number of iterations required in obtaining a stable resonance frequency increases with the increment in the drive level. The number of iterations required depends on the convergence criteria. The convergence criterion here is defined as a function of the shift in the resonance frequency. The FE solution is converged when the frequency shift in the resonance frequency between any consecutive iteration is less than 0.5 Hz. Thus, for a 40 MHz resonator the maximum allowable difference in the resonance frequency shift between consecutive iterations is less than 0.0125 ppm. The number of iterations required to obtain the DLD at the various drive level is shown in Table 1.

Here, the FE simulation is carried out by including the material losses for all the different rotated cut angles of quartz resonator (Lamb and Richter, 1966) and the gold electrodes (International critical tables of numerical data, 1929). Also, the electrical conductivity for each rotated quartz cuts is considered (Lee et al., 2004). Thus, the FE simulations for predicting DLD are carried out only for the intrinsic losses in quartz and electrodes. No external damping parameters and loss factors are taken into account.

Table 1
No. of iterations required to obtain a stable solution.

Drive level (V)	No. of iterations required
0.0001	0
0.001	0
0.01	1
0.10	1
0.30	2
1.0	3
5.0	6
8.0	10
10.0	12

3.1. DLD in various AT-Cut quartz resonators

Frequency response analyses for various AT-cut resonators are carried out for the dimensions shown in Fig. 1. The "small sample" and "large sample" mentioned in Fig. 1 are abbreviated as "SS" and "LS" in Figs. 5–8. Fig. 2 shows the mesh plot used for AT-cut quartz resonators. The element distribution consists of two layers of element through the thickness. An aspect ratio rule for the number of elements along the width and length is used. This rule came from our observations that the largest number of half waves of resonant modes follow a/b and c/b ratios. ($2a$ = length, $2b$ = thickness, $2c$ = width). If a/b ratio is 10, then the number of flexural half waves is about 10. We have used two or more elements per half wave. The element type used for the 3-D FEM analysis is the 27-node brick element. The same aspect ratio rule is followed for the finite element mesh for different cut angles of quartz resonators mentioned in this paper. Fig. 3 shows a typical thickness shear mode obtained for the resonators. Fig. 4 shows the displacement amplitude at a material point located at the electrode center versus the driving frequency. The curve is obtained by a linear frequency response analysis at a drive level of 0.0001 V. When the drive level is increased, not only does the peak response increase in magnitude, the frequency at the peak response also changes. This is the DLD effect on the resonance frequency.

The simulation and the experimental results obtained for the flat blank resonators are shown in Figs. 5–8. Drive level dependency can be described in terms of the frequency change versus drive levels. The drive level can be expressed either as the voltage drive, electric current density, electric field, or power density. A useful drive level expression should be one which takes into account the resonator parameters such as its size, electrode dimensions and resonator Q because we have found experimentally that these parameters affects the resonator DLD.

(a) *Voltage drive level:* The graph in Fig. 5 shows the DLD of AT-cut resonators with respect to the voltage drive level (volts). It can be seen that the FE simulated curves follow the same trend as the experimental results for different samples of the resonators. In order to take into account the resonator resistance and dimensions, we further plot the DLD in terms of the electric field, current density and power density.

(b) *Electric field drive level:* The graph shown in Fig. 6 shows the frequency shift in ppm versus electric field (V/m) drive level for both the FE simulated results and experimental results. We see that the experimental curves and FE curves behave similarly. These curves give a better representation of the DLD because the thickness of these resonators is taken into account.

(c) *Current density drive level:* Another representation of the DLD is in terms of the current density drive level in A/m^2. The current density drive level is calculated by integrating the surface current density over the electrode region for a fixed drive level voltage. The current density calculated for different drive level voltage was then plotted against the shift in the frequency for each respective drive level voltage. Thus, the DLD in terms of current density drive level represent the shift in the resonant frequency with respect to the electric field generated due to an applied drive level voltage. The graph shown in Fig. 7 shows the comparison of experimental curves with the FE simulated curves. The comparison shows a good agreement of the FE simulation results with the measured data.

(d) *Power density:* The graph shown in Fig. 8 shows the DLD in terms of the power density (W/m^3). Here, the simulation results and the experimental results show the same frequency drift, and the simulation results follow the same

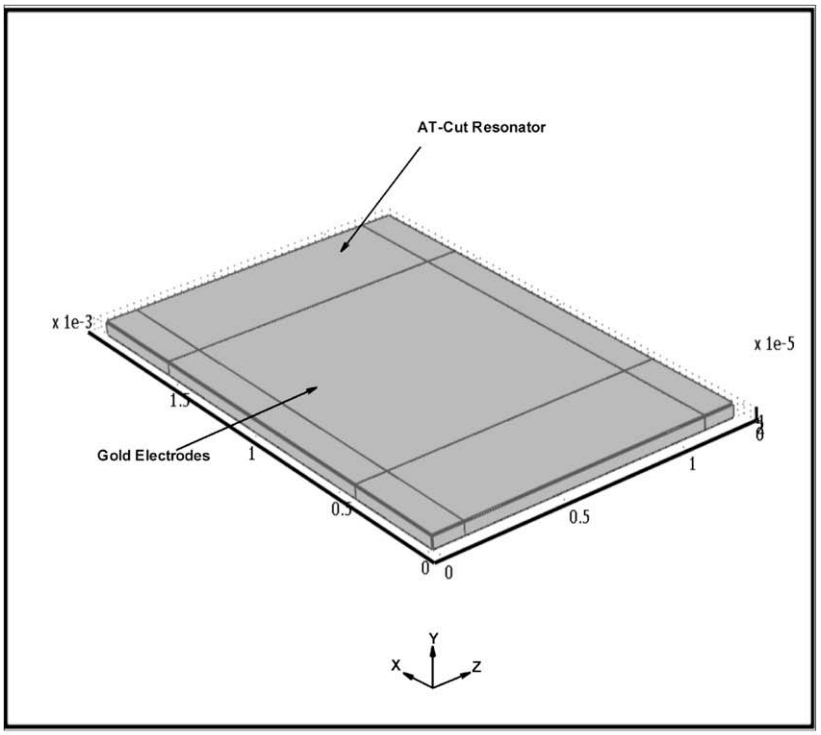

	Dimensions of Different Samples	X1 (microns)	X2 (microns)	X3 (microns)
AT-Cut	Small Sample @20 MHz	1996	85	1323
	Large Sample @ 20 MHz	5400	85	1604
	Small Sample @48 MHz	1996	32.25	1200
Electrode Dimension	Small Sample @ 20 MHz	1100	0.1	1000
	Large Sample @ 20 MHz	2700	0.1	1000
	Small Sample @48 MHz	1200	0.1	700

Fig. 1. Model and dimensions of various AT-Cut resonators.

trend as that of the experimental results. The frequency shift for all the samples except for the "SS-48 MHz" shows a very good agreement with the experimental results. The FE model is simulated using only the acoustic viscosity loss parameters, and energy dissipation due to the mountings is not taken into consideration. Hence, the magnitude of the power density simulated is different from the experimental power density. Since the power density is the product of the current density and voltage drive level, the resulting plot give us a linear representation of the DLD effect. The DLD curve plotted with respect to power density helps us in generalizing the DLD for various resonator size having different frequency spectrums. It serves as a universal parameter for the DLD as it takes into account all the resonator parameters.

3.2. DLD in SC-Cut quartz resonators

Circular SC-cut quartz resonators are studied. Fig. 9 shows the dimensions for the resonator. The simulation and the experimental results obtained for DLD are plotted (Fig. 10) as a function of the universal parameter: power density. Here, the FE simulation curve shows the same trend as the experimental curve.

3.3. DLD in BT-Cut quartz resonators

The DLD in a BT-cut quartz resonator is also studied and compared with the experimental data. The dimensions of resonator used for the experimental and analytical analyses are shown in Table 2.

The DLD versus power density is shown in Fig. 11. The DLD curves for both the FE simulation and experiment follow a negative slope with a good agreement. The FE-simulation could predict both positive DLD with respect to power density (AT- and SC-cut resonators) and, now, negative DLD with respect to power density. This further demonstrates the validity of the FE model.

3.4. DLD in doubly rotated quartz resonators

We now use our FE model for the study of DLD in various doubly rotated cut in order to seek a cut which yields a small DLD, and simultaneously retains the desirable frequency–temperature (f–T) behavior of the AT-cut resonators. Hence, the quartz crystal cuts are rotated about the x_3-axis with an angle varying from 0° to 22° while the angle rotated with respect to the x_1-axis is kept relatively fixed at about 34.93°. The dimensions used for these doubly rotated cuts are given in Table 3.

The first set of data corresponds to quartz crystal rotated about x_3-axis at an angle of 9° and 12°, and the x_1-axis rotated at 34.91° and 34.73°, respectively. The simulation results and the experimental results are shown in the DLD versus power density graphs below. Fig. 12 shows that a doubly rotated cut having an angle of $x_3 = 12.0°$ has a very low DLD response.

Three figures (Figs. 13–15) shows the simulated DLD versus power density curves for double rotated cuts of quartz with phi varying from 0° to 22° for theta equal to 34.93°. The aspect ratio

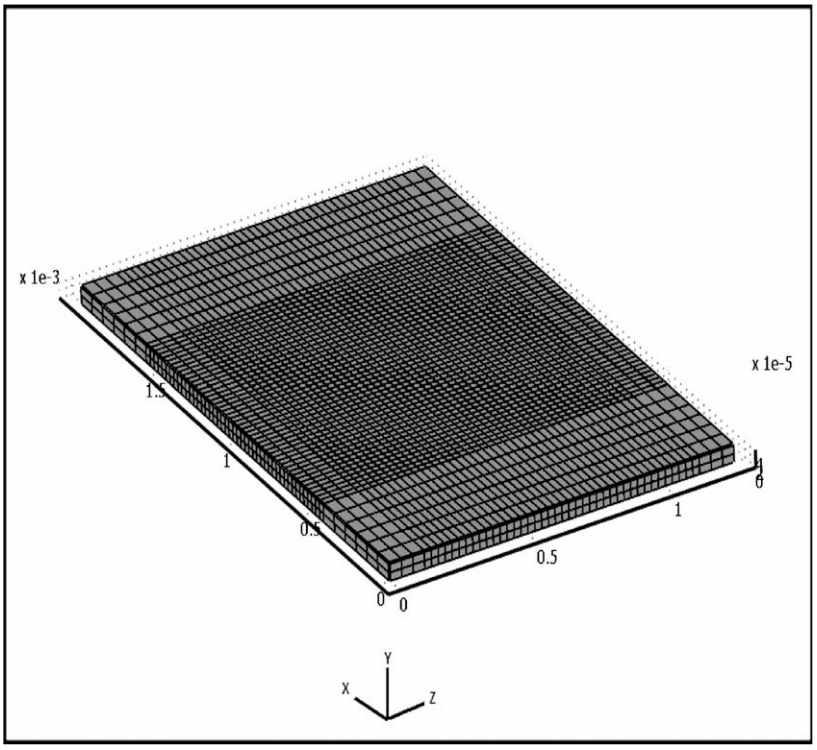

Fig. 2. 3-D FE mesh plot for AT-Cut resonator.

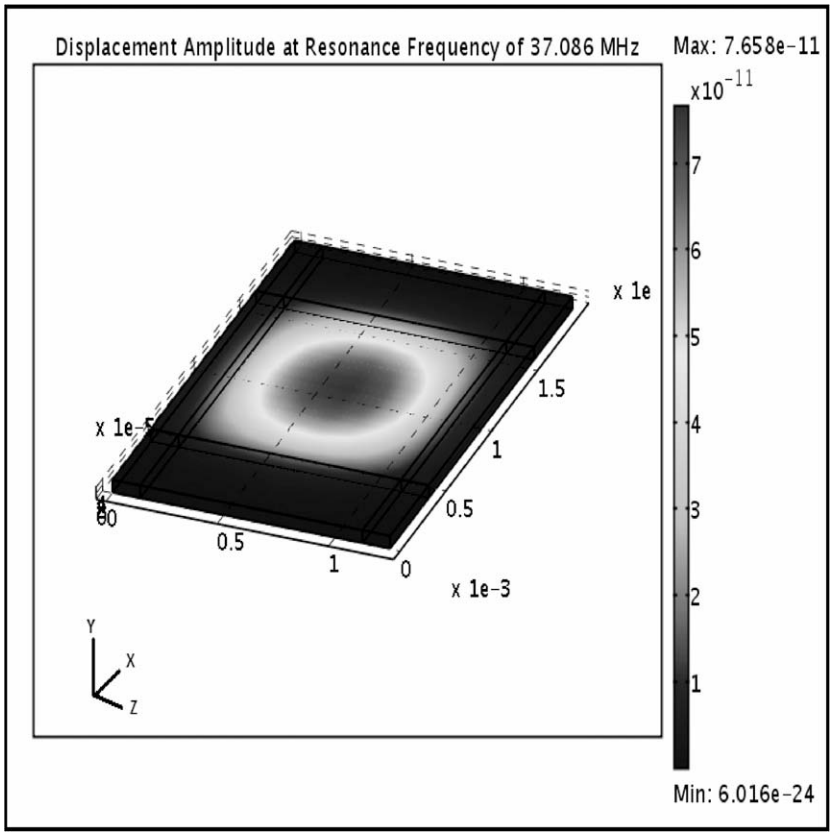

Fig. 3. Thickness shear mode for 40 MHz AT-Cut resonator.

selected for these cut angles is based on the frequency spectrum analysis carried out in Section 4. Figs. 13–15 show the DLD curves with the cut angle phi varying from 1° to 7°, 8° to 14° and 15° to 22°, respectively. The graphs show that the cut angles of phi equal to 8° and 9°, and theta equal to 34.93° have the lowest DLD. It has also been shown experimentally that the cut angle with phi equal

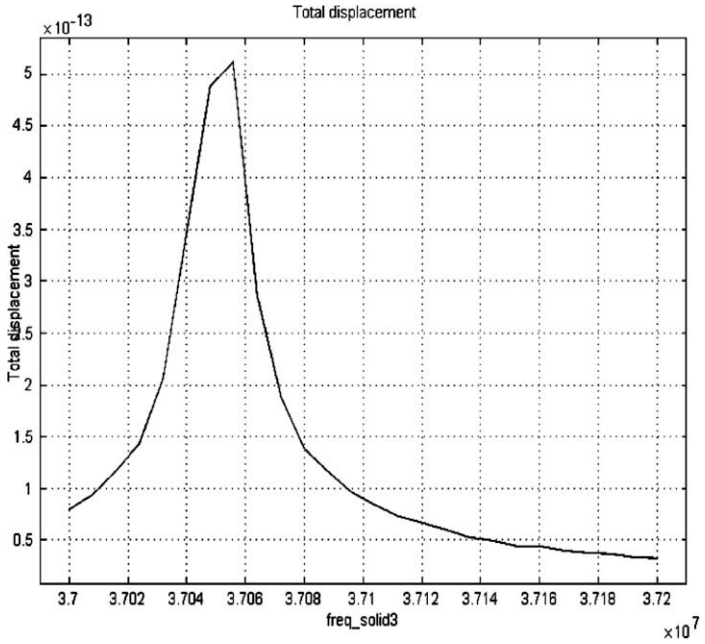

Fig. 4. Displacement amplitude plot in the vicinity of thickness shear mode frequency for AT-Cut resonator.

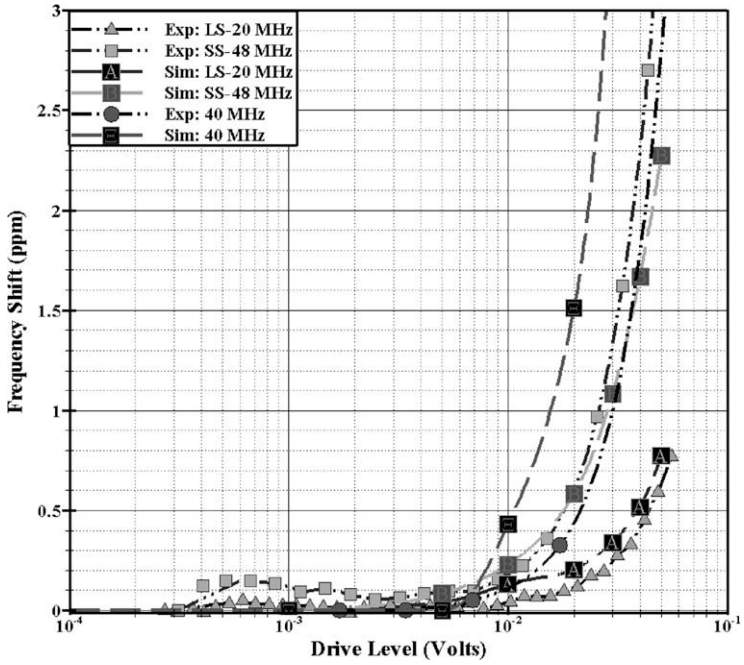

Fig. 5. DLD versus voltage drive level for AT-Cut resonators.

to 8° and theta equal to 34.93° is also a temperature stable cut. The most DLD sensitive cut is for phi equal to 19.0° and theta equal to 34.93°.

The DLD versus power density curves are relatively straight lines. At a given power density we can find the slope of the curve. We define this slope as the frequency shift gradient. A graph of the frequency shift gradient versus the cut angle will allow us to find the cut angles which yield small DLD effects. The next graph (Fig. 16) shows a plot of the frequency shift gradient obtained from the power density curve versus the cut angle phi.

4. Effect of spurious mode on drive level dependence of quartz resonators

The aspect ratio used for all FE simulation until now for all the different cut angles is 45.885. This aspect ratio is based on the experimental work carried out for doubly rotated cut rotated about the x_3-axis with an angle of 9.0° and x_1-axis rotated about 34.91°. However, for different aspect ratios and for different cut angles the energy of the trapped thickness shear mode varies due to the interaction of the spurious modes with that of the thickness shear

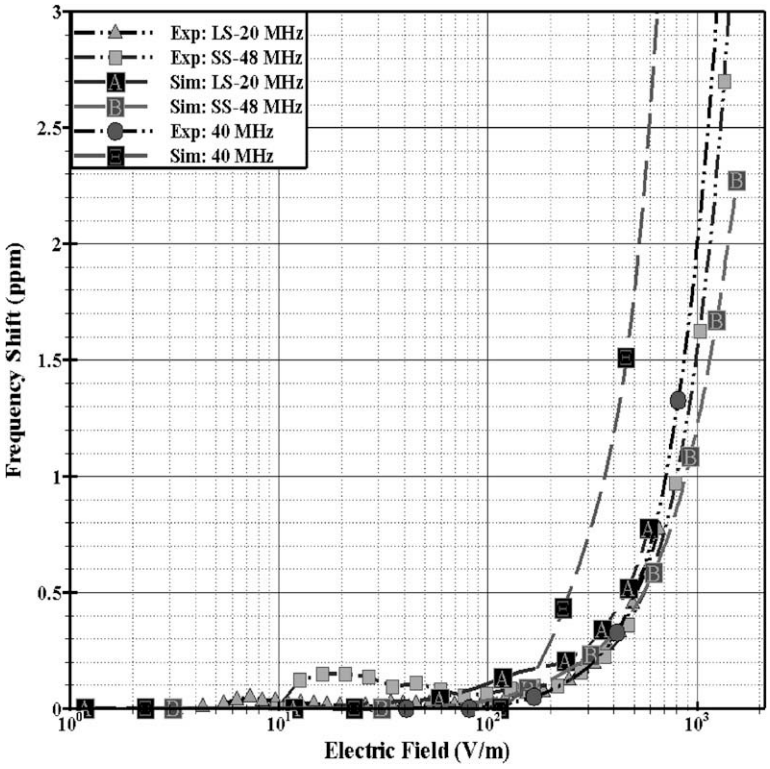

Fig. 6. DLD versus electric field for AT-Cut resonators.

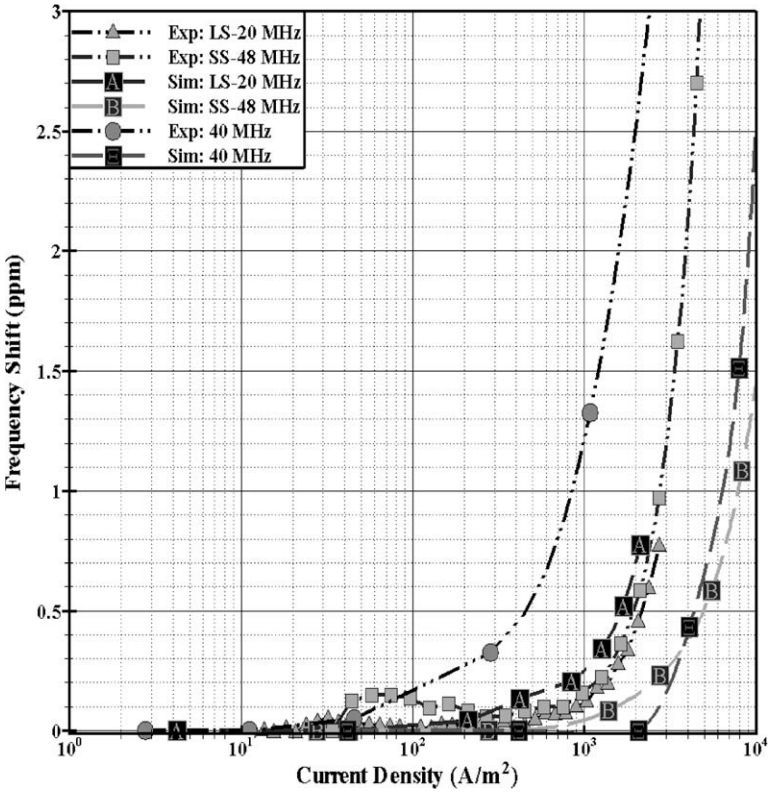

Fig. 7. DLD versus current density for AT-Cut resonators.

mode. Since all the FE simulations for DLD discussed in the above section for doubly rotated cuts were carried out on the basis of one fixed aspect ratio, a detailed study of the effect of spurious modes on the drive level dependency in quartz resonators is required.

In order to study to the effect of different spurious modes on drive level dependency, the first step is to obtain the acoustic behavior for different doubly rotated quartz cuts with varying aspect ratio. The aspect ratio is defined here as the

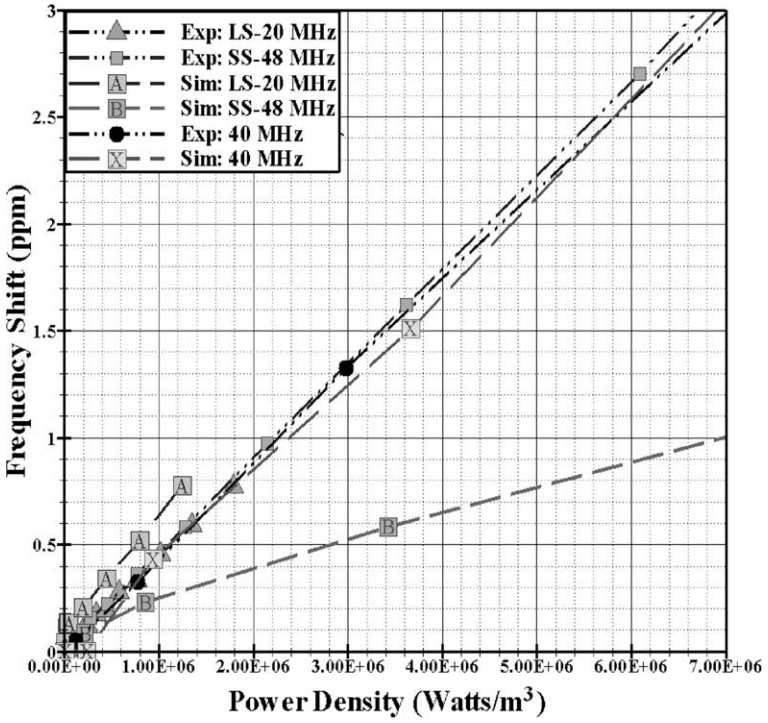

Fig. 8. DLD versus power density for AT-Cut resonators.

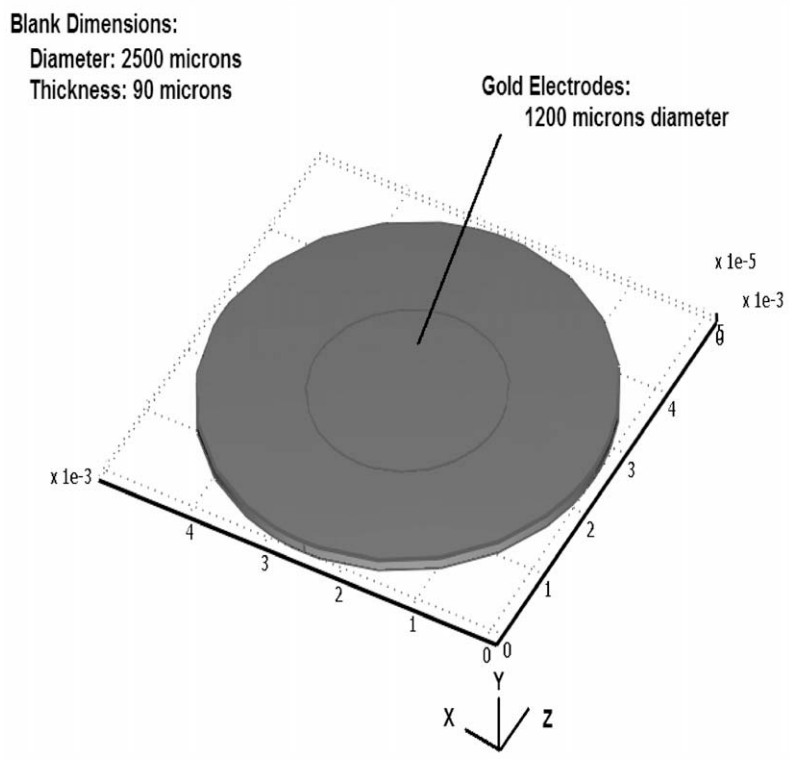

Fig. 9. Model of SC-Cut quartz resonator.

ratio of the resonator length to its thickness dimension. The acoustic behavior is studied from the frequency spectra obtained by performing free vibration analysis. The frequency spectrum enables to determine the thickness shear mode which is affected by the spurious mode for different aspect ratios. Fig. 17 shows one of the frequency spectra obtained for doubly rotated cut having and with aspect ratio varying from 45.5 to 46.5.

The standard notations used in all the frequency spectrum graphs are as follows:

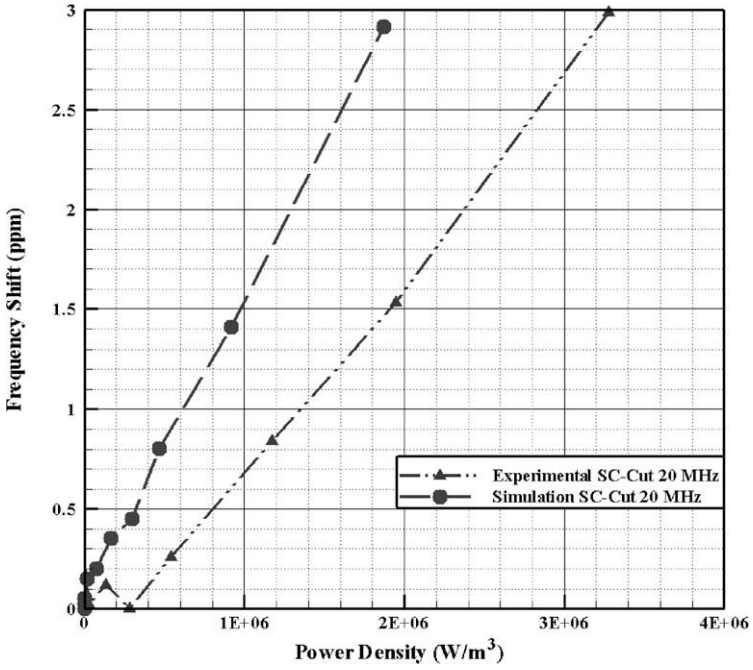

Fig. 10. DLD versus power density for SC-Cut resonators.

Table 2
BT-Cut resonator dimensions.

	x_1 (microns)	x_2 (microns)	x_3 (microns)
BT-cut resonator dimension	2800	50	1400
Electrode dimensions	1600	0.1	1000

Table 3
Doubly rotated cut resonator dimensions.

	x_1 (microns)	x_2 (microns)	x_3 (microns)
Doubly rotated cut resonator dimensions	2000	44	1200
Electrode dimensions	1200	0.1	1000

(a) "Square" notation is used to represent the modal branch with high energy and current i.e. the fundamental thickness shear mode.

(b) "○" notation is used to represent the modal branch with high current only.

(c) "Δ" notation is used to represent the modal branch with high energy only.

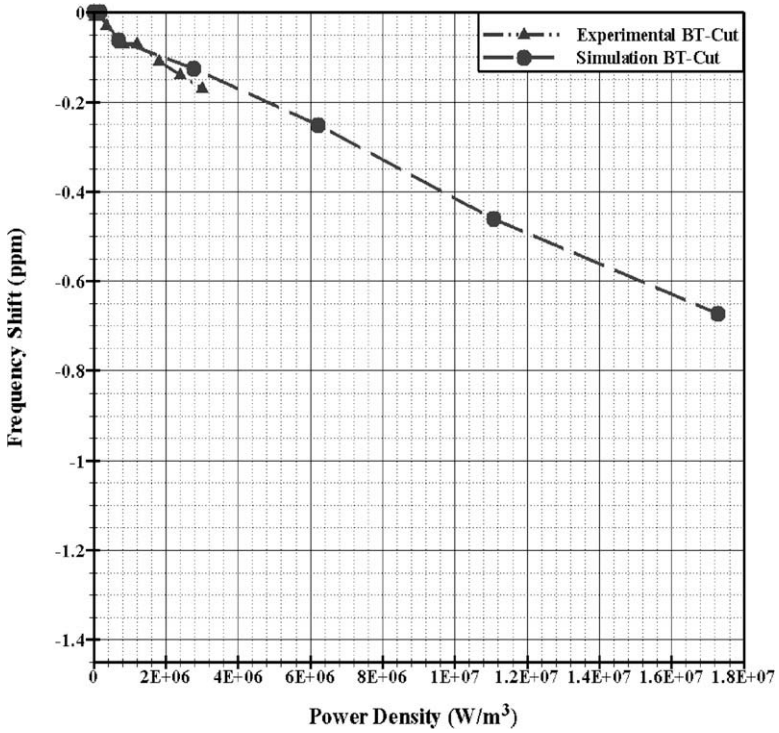

Fig. 11. DLD versus power density for BT-Cut quartz resonators.

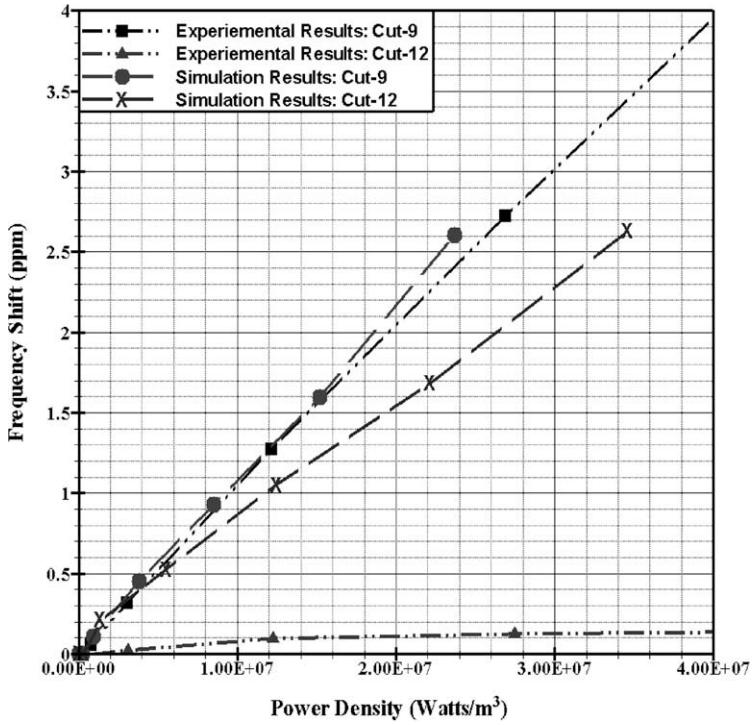

Fig. 12. Comparison of experimental versus FE results for Cut-9 and Cut-12.

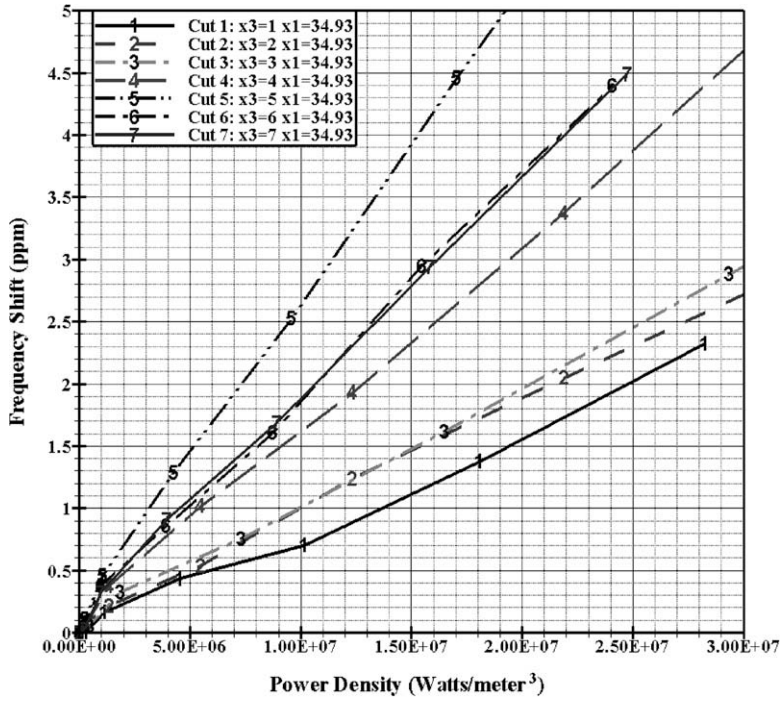

Fig. 13. DLD versus power density curves for doubly rotated cut of quartz with phi varying from 1° to 7°.

(d) "×" notation is used to represent the modal branch for other modes.

The top graph in the frequency spectrum shows the resonant frequencies versus the aspect ratio. We see that there is an interaction of the spurious mode with that of the thickness shear mode for an aspect ratio of 45.92.The middle graph shows the electrode current relative to unit eigenvectors of the eigenvalue analyses. It can be observed on comparison the top and the bottom graph that there is a drop in the electrode current relative to unit eigenvectors (eigen modes) at the same aspect ratio of 45.92. Also, there is a drop in the electrode current for an aspect ratio of 45.885 indicating the presence of spurious mode. The bottom graph represents the ratio of trapped thickness shear mode energy to total energy which shows that there is an energy drop for aspect ratio of 45.92 and 45.885. Thus, the previous DLD analysis carried out in

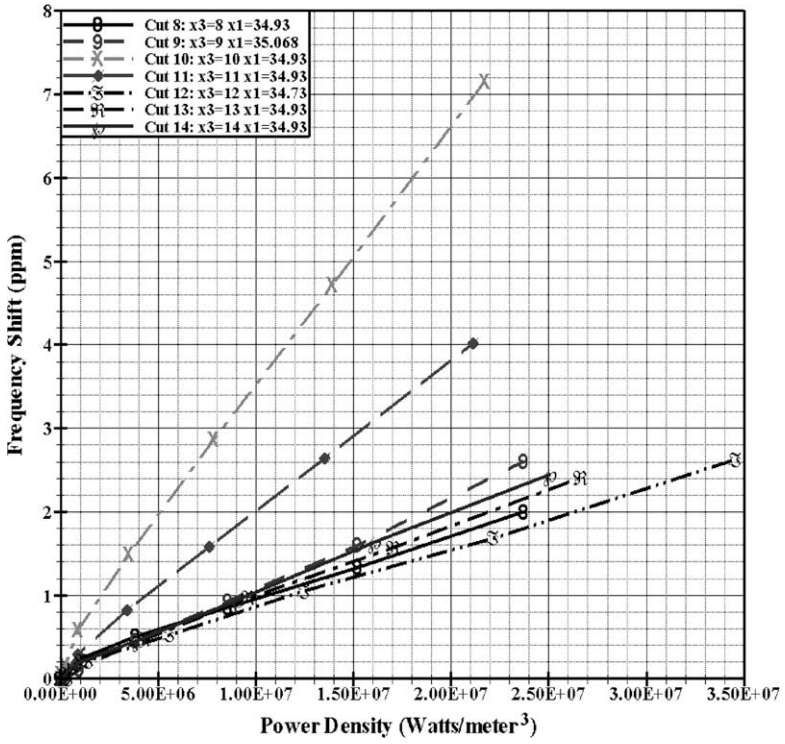

Fig. 14. DLD versus power density curves for doubly rotated cut of quartz with phi varying from 8° to 14°.

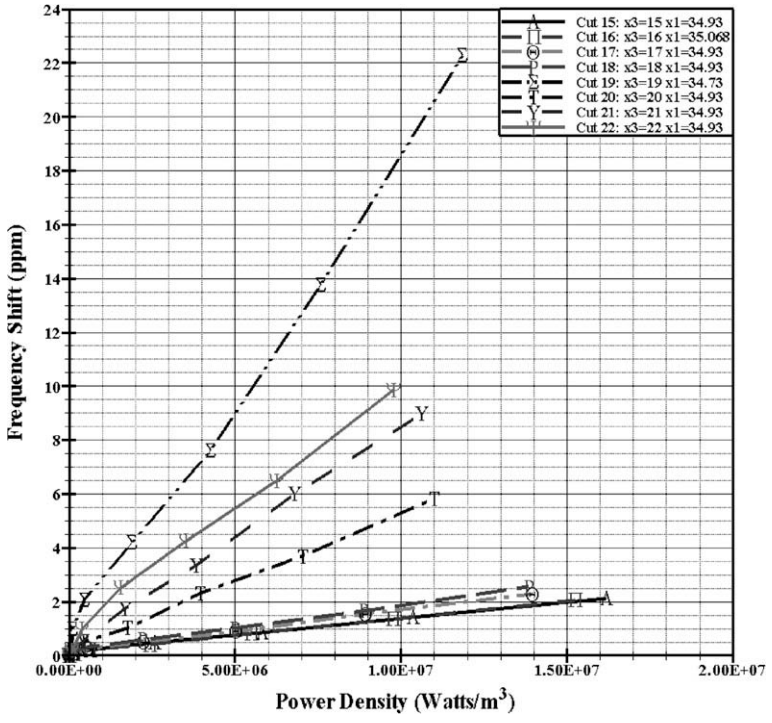

Fig. 15. DLD versus power density curves for doubly rotated cut of quartz with phi varying from 15° to 22°.

the previous section for this cut angle is affected by the spurious mode. The frequency spectra thus help in the selection of a clean aspect ratio of 45.80 which is not affected by the spurious modes.

In the second step, DLD analysis is performed using the iterative procedure mentioned in Section 2 for the clean aspect ratio of 45.80 and for aspect ratio of 45.92 which is affected by the spurious modes. The graph in Fig. 18 shows the comparison of the DLD curves in terms of power density for aspect ratio of 45.80 and 45.92. It can be observed that there is significant increase in the drive level sensitivity for aspect ratio of 45.92 (affected by spurious mode) as compared to that for clean aspect ratio of 45.80. Thus, it can be concluded that the presence of spurious mode does change the drive level dependence of the quartz resonators. However, it should be noted that the effect of spurious modes on the

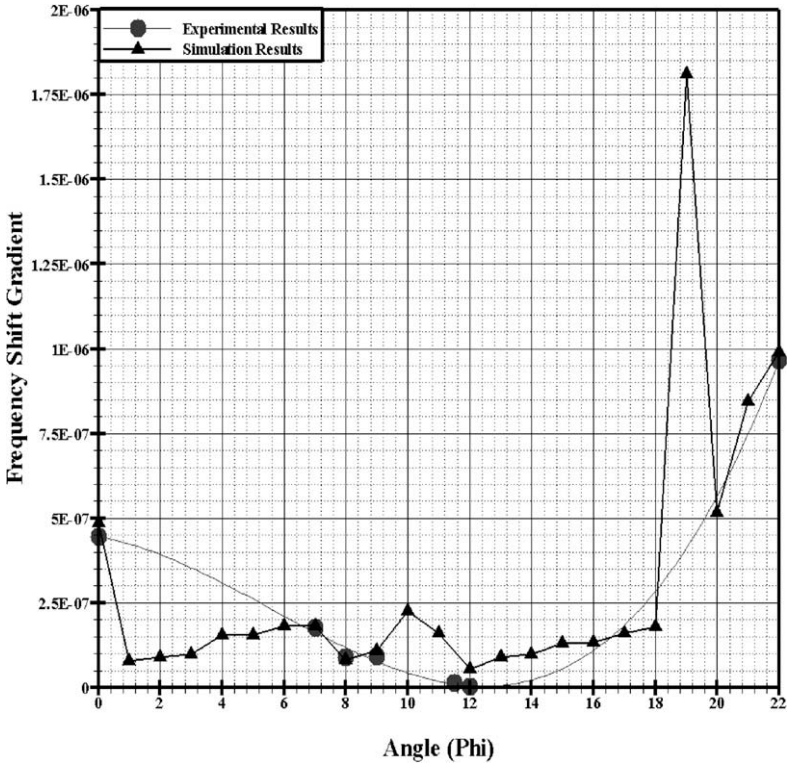

Fig. 16. Frequency shift gradient due to DLD versus cut angle phi.

drive level dependency for different cuts is different. Thus, in order to characterize the effect of aspect ratio on the DLD for different cuts, frequency spectrum analysis is carried out for all the cut angles varying for 0°, 3°, 6°, 9°, 10°, 12°, 15°, 18°, 19°, 20° and 21°. Based on the frequency spectrum analysis a clean aspect ratio of 45.88, 45.86, 45.70, 45.88, and 45.90 is selected for cut angles of 3°, 6°, 9°, 12°, and 15° degrees, respectively. Drive level dependency of all these cut angles for clean aspect ratio is carried out. Figs. 13–15 shows the drive level dependency of all these cut angles with respect to the clean aspect ratio. It can be now seen from Fig. 16 that the predicted DLD for cut angle having 9 and 12 degrees is in good agreement with the measured results when compared with the FE predicted results in Fig. 12. Thus, one of the main reasons in the discrepancy between the FE predicted results and the experimental results can be attributed to the effect of aspect ratio.

5. Drive level dependency and quality factor

The quality factor Q is one of the important factors in deciding the stability of quartz resonators. In order to obtain a relationship between the Q and the drive level dependence of a quartz resonator, an "energy sink approach" is integrated into the DLD FE model (Yong et al., 2005). This approach takes into consideration the energy losses due to the mountings by assuming a semi-infinite boundary at the mountings. The relationship between the quality factor and the drive level dependence helps us understand the resistance which changes the DLD curve and the quality factor. As the quality factor decreases, the resistance increases. Since the power density takes into consideration the resistance, it is the most suitable parameter for describing the DLD effect in quartz resonators.

A FE simulation is carried out with respect to the experimental setup used in determining the quality factor of the AT-cut quartz resonator as a function of the position of a point probe.

The experimental setup is shown in Fig. 19 along with the locations of the point probe (numbered 1–4). When the point probe is moved from locations 1–4, it interferes with the displacement distribution of the resonator; energy is dissipated via the probe, and the resonator Q drops.

The dimensions of the AT-Cut quartz resonator used are given in Table 4:

The simulation results are carried out by considering a semi-infinite boundary condition at the probe position; hence all the energy dissipated from the quartz resonator is being absorbed at this particular boundary interface. The drop in Q due to the increase in the resistance obtained from experimental and simulation results is shown in graph of Fig. 20. The graph shows that the motional resistance increases (with a corresponding decrease in Q) as the position of the probe is moved towards the electrode region of the resonator.

Fig. 21 shows the simulation results and the experimental Q for the resonator at different probe positions. The simulation results gives the lowest possible Q for the 20 MHz AT-Cut quartz resonator mounted on supports because of the semi-infinite boundary conditions assumed at the mountings and at the probe. The semi-infinite boundary conditions absorb all energy incident upon them. In the experiment, some energy is reflected back from the mountings and the probe.

Fig. 22 above shows the drop in the power density as the position of probe is moved from the resonator edge to the electrode edge. The drop in the power density corresponds to the drop in resonator Q. The result shows a very interesting trend for the DLD and the Q-factor. It can be observed that for no change in the Q-factor value the power density requirement for the quartz resonator remains constants. This implies that the slope of the power density curve from probe position 1 to probe position 2 almost tends to zero, which indicates that the quartz resonator is DLD stable. However, once the probe is moved from position 2 to position 4 there was a drop in the Q-factor value indicating that the quartz

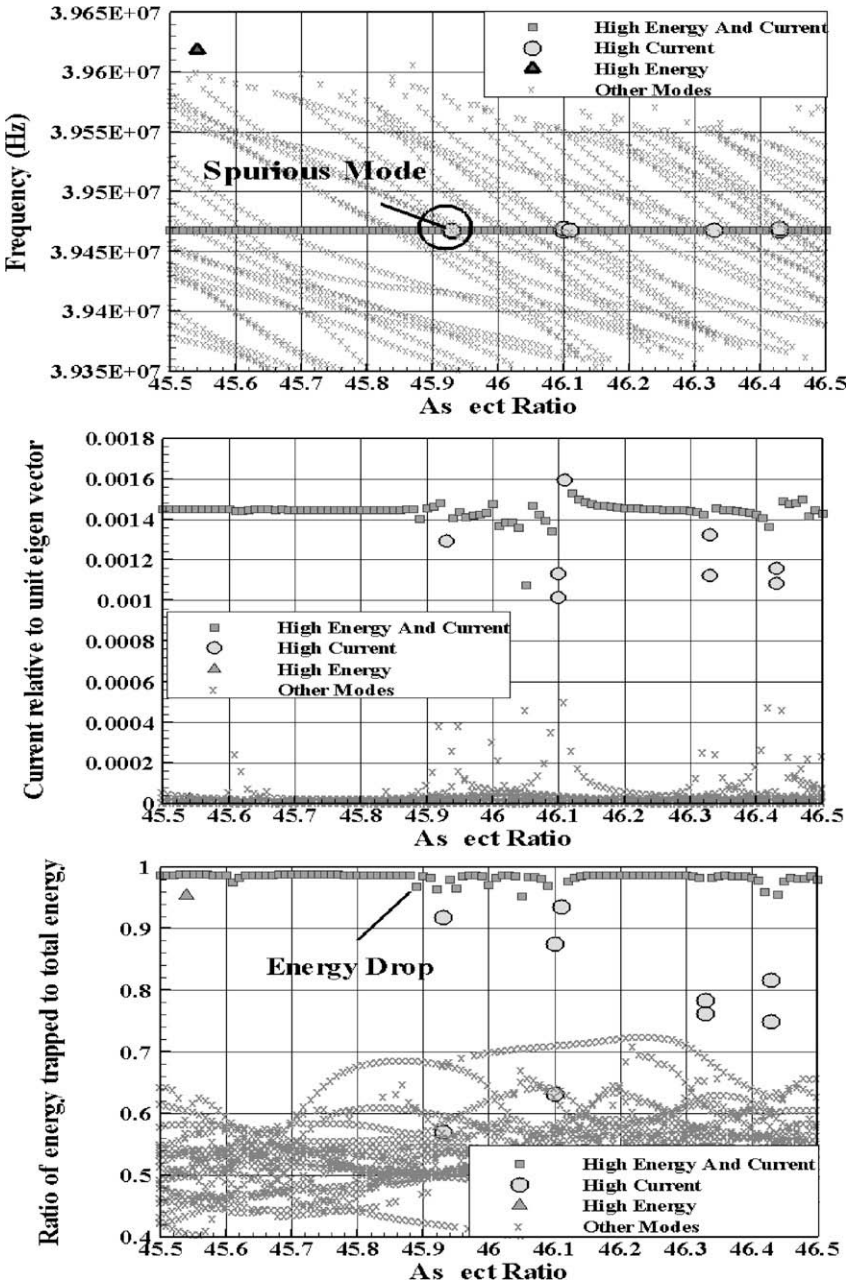

Fig. 17. Frequency spectrum for doubly rotated quartz cut having $\phi = 19°$ and $\theta = 34.93°$.

resonator becomes more unstable. The drop in the Q-factor value is traced by the power density curve. The slope of the power density curve increases with the drop in the Q-factor value resulting in a more sensitive DLD quartz resonator. The power requirements for a low Q value quartz resonator decrease but at the same time even a very small fluctuation in the drive level power can make the resonator more unstable. Thus, the Fig. 22 shows that the Q-factor and the DLD are linearly dependent on each other.

Also, experimental results show that the soft probe used for the measurement of Q-factor increases the motional resistance of the blank. This could be one of the main reason for the difference between the experimental and FE simulation results. The effect of the probe size on the Q-factor and the motional resistance is extensively studied in (Yong et al., 2005). The studies shows that even a small difference in the probe size can affect the motional resistance of the blank. Hence, a further investigation of the effect of probe size on the DLD is suggested.

6. Effect of air damping on DLD and Q-factor

The Q of a quartz resonator is greatly affected by air damping which results in a large difference between the Q in air and vacuum. Hence experiments are carried out on 48 MHz AT-Cut resonator in order to understand the influence of air damping on DLD and Q. The dimensions for the 48 MHz AT- Cut resonator are given in Table 5.

The experiments were carried out in a vacuum chamber and in normal atmospheric conditions with supports to calculate the change in the DLD and Q.

The measurement results show that the Q measured in vacuum is almost 1.5 times higher than that measured in normal

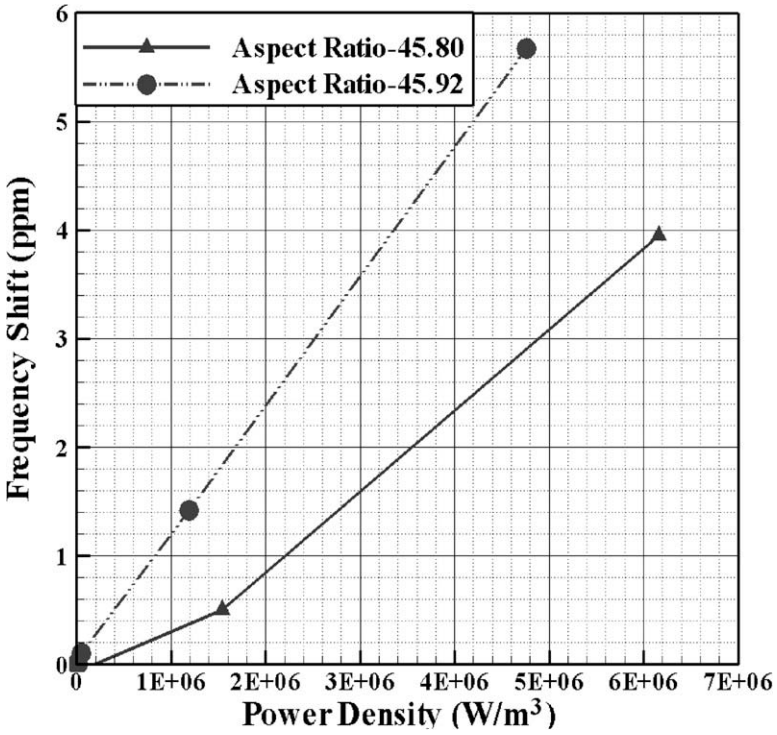

Fig. 18. DLD versus power density curves for doubly rotated quartz cut having $\phi = 19°$ and $\theta = 34.93°$ for aspect ratios of 45.80 and 45.92.

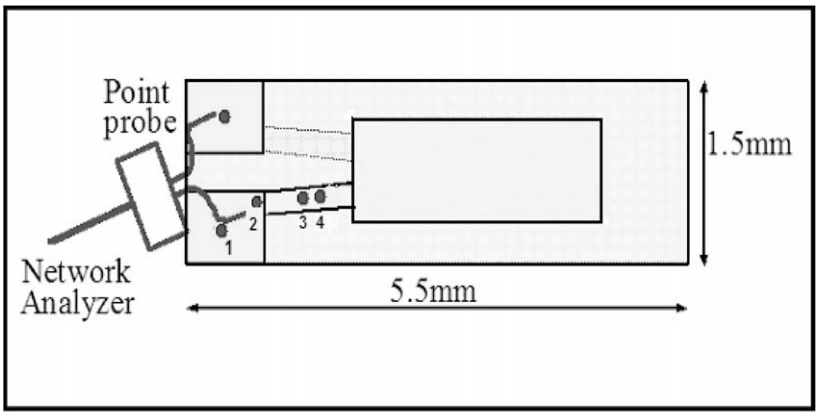

	X1 length, (microns)	X2 thickness, (microns)	X3 width, (microns)
Blank dimensions	5500	80	1500
Gold electrode dimensions	2700	0.1	1000

Fig. 19. Experimental setup for the determination of resonator Q as a function of the position of point probe.

atmospheric conditions. Although there was a significant drop in the Q due to air damping, the DLD is observed to be not much affected by the air damping. The result shows that the Q does not have significant effects on the DLD.

Table 4
AT-cut blank dimensions used for determining relationship between DLD and quality factors.

	x_1 (microns)	x_2 (microns)	x_3 (microns)
AT-cut blank dimensions	5500	80	1500
Electrode dimensions	2700	0.1	1000

Table 5
AT-cut blank dimensions.

	x_1 (microns)	x_2 (microns)	x_3 (microns)
Blank	1996	32.2	1150
Gold electrode	1150	0.1	800

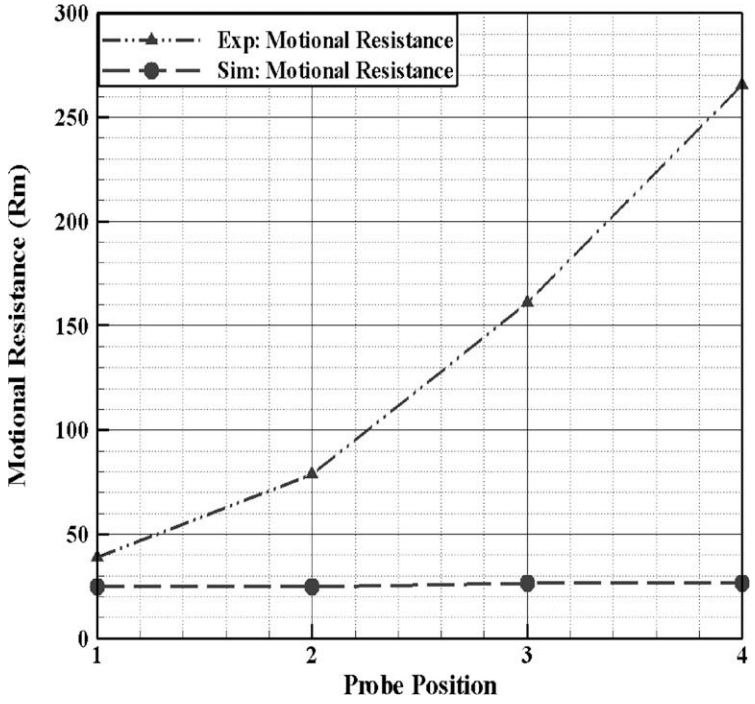

Fig. 20. Motional resistance of the resonator as a function of the probe position for the experimental setup of Fig. 22.

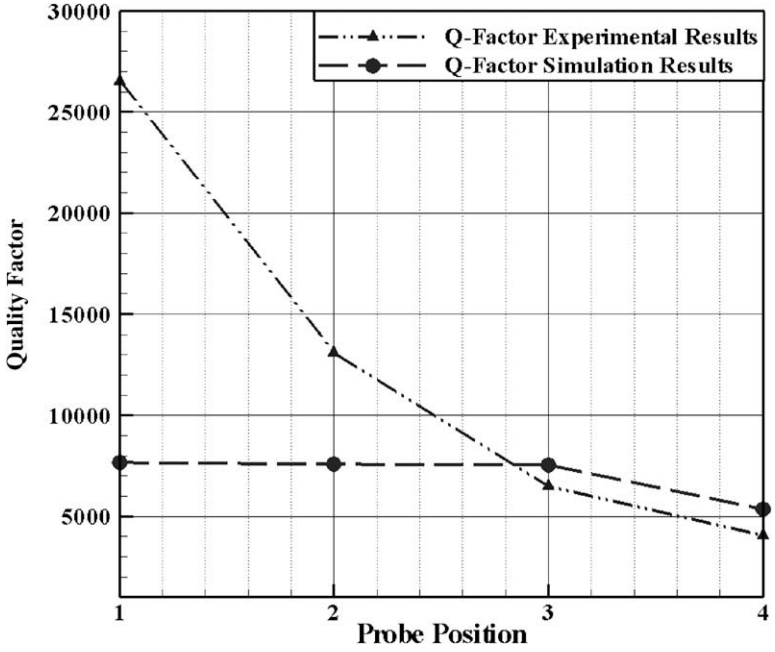

Fig. 21. Resonator Q versus the probe position.

7. Summary

The drive level dependence of the resonance frequency of quartz resonators (DLD) is caused mainly by the third-order elastic constants. Any variation for a particular value of third-order elastic constant necessitates a change in the overall symmetry of the quartz. Thus, the results obtained for different rotated quartz cut angles represent the variation of the third order elastic constants with respect to DLD. The results obtained from the finite element models for predicting the DLD compare reasonably well with the experimental data for different crystal cuts of quartz. Hence the FE models could be employed for predicting the DLD in new cuts of quartz. The jump in DLD at $\phi = 10^\circ$ could be mainly due to a stronger coupling between the third-order elastic constants and the strain field caused due to the drive level. The FE simulations for different doubly rotated cuts show that the lowest DLD could be obtained for cut angle with $\phi = 8^\circ$ and $\theta = 12^\circ$. The study shows that the power density applied to the quartz resonator best describes its DLD. The power density is the best parameter for defining the DLD. The FE predictions of the resonator Q shows the same

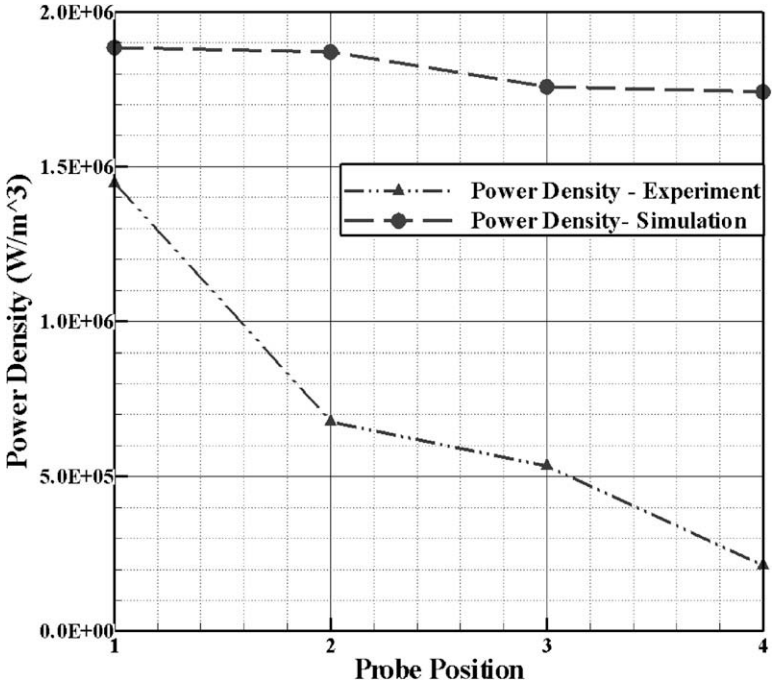

Fig. 22. Power density versus probe position.

trend as the measured Q. A decrease in the resonator Q decreases the DLD, however the effect is weak.

References

Gagnepain, J.J., Poncot, J.C., Pegeot, C. 1977. Amplitude frequency behavior of doubly rotated quartz resonators. In: Proceedings of 31st Annual Symposium on Frequency Control, US Army Command, Fort Monmouth, New Jersey, pp. 17–22.

Warner, A.W., 1959. Interim Reps. Bell Telephone Lab., pp. 10–11.

Wood, A.F.B., Seed, A., 1967. Activity dips in AT-Cut crystals. In: Proc. of 21st Annual Symposium on Frequency Control, pp. 420–435B.

Tiersten, H.F., 1974. Nonlinear electrostatic equations cubic in small field variables. Journal of Acoustical Society of America, 660–666.

Tiersten, H.F., 1975. Analysis of trapped-energy resonators operating in overtones of coupled thickness shear and thickness twist. In: Proc. of 28th Annual Symposium on Frequency Control, p. 44.

Tiersten, H.F., 1975. Analysis of intermodulation in thickness-shear and trapped energy resonators. Journal of Acoustical Society of America 57 (3), 667–681.

Yong, Y.K., Patel, M.S., Hou, J., Lam, C.S., 2007. Piezoelectric resonators with mechanical damping and resistance in current conduction. Science in China Series G: Physics, Mechanics and Astronomy 50 (5), 650–672.

Lamb, J., Richter, J., 1966. Anisotropic acoustic attenuation with new measurement for quartz at room temperatures. Proceedings of the Royal Society 293A, 479–492.

Hellwedge, K.H., Hellwedge, A.M., 1966. Numerical data and functional relationships in science and technology. Landolot-Bornstein, vol. 1. Springer, Berlin.

Thurston, R.N., McSkimin, H.J., Andreatch Jr., P., 1966. Third-order elastic constants of quartz. Journal of Applied Physics 37, 267.

Lee, P.C.Y., Liu, N.H., Ballato, A., 2004. Thickness vibrations of piezoelectric plates with dissipation. IEEE Transactions UFFC 51 (January), 52–62.

International Critical Tables of Numerical Data, Physics, Chemistry and Technology, 1929. International Critical Tables of Numerical Data, Physics, Chemistry and Technology, first edition, vol. 5. Prepared under Int. Research Council of National Academy of Sciences, USA, pp. 6–7.

Yong, Y.-K., Patel, M., Tanaka, M., 2005. Estimation of quartz resonator Q and other figures of merit by an energy sink method. In: Proceedings of the 2005 IEEE International Frequency Control Symposium.